PLOS Biology

RESEARCH ARTICLE

Reactivation of previous decisions repulsively biases sensory encoding but attractively biases decision-making

Minghao Luo[1,2☯], **Huihui Zhang**[1,2,3,4☯*], **Fang Fang**[1,2,3,5*], **Huan Luo**[1,2,5*]

1 School of Psychological and Cognitive Sciences and Beijing Key Laboratory of Behavior and Mental Health, Peking University, Beijing, China, **2** PKU-IDG/McGovern Institute for Brain Research, Peking University, Beijing, China, **3** Peking-Tsinghua Center for Life Sciences, Peking University, Beijing, China, **4** Institute for Artificial Intelligence, Peking University, Beijing, China, **5** Key Laboratory of Machine Perception (Ministry of Education), Peking University, Beijing, China

☯ These authors contributed equally to this work.
* huihuizhang@pku.edu.cn (HZ); ffang@pku.edu.cn (FF); huan.luo@pku.edu.cn (HL)

OPEN ACCESS

Citation: Luo M, Zhang H, Fang F, Luo H (2025) Reactivation of previous decisions repulsively biases sensory encoding but attractively biases decision-making. PLoS Biol 23(4): e3003150. https://doi.org/10.1371/journal.pbio.3003150

Academic Editor: Uta Noppeney, Radboud Universiteit Donders Institute for Brain Cognition and Behaviour, NETHERLANDS, KINGDOM OF THE

Received: October 14, 2024

Accepted: April 2, 2025

Published: April 23, 2025

Data availability statement: Data supporting main findings of the study are available at https://osf.io/c7dwp/.

Funding: This work was supported by the Science Fund for Creative Research Groups of the National Natural Science Foundation of

Abstract

Automatic shaping of perception by past experiences is common in many cognitive functions, reflecting the exploitation of temporal regularities in environments. A striking example is serial dependence, i.e., current perception is biased by previous trials. However, the neural implementation of its operational circle in human brains remains unclear. In two experiments with electroencephalography (EEG)/magnetoencephalography (MEG) recordings and delayed-response tasks, we demonstrate a two-stage 'repulsive-then-attractive' past–present interaction mechanism underlying serial dependence. First, past-trial reports, instead of past stimuli, serve as a prior to be reactivated during both encoding and decision-making. Crucially, past reactivation interacts with current information processing in a two-stage manner: repelling and attracting the present during encoding and decision-making, and arising in the sensory cortex and prefrontal cortex, respectively. Finally, while the early stage occurs automatically, the late stage is modulated by task and predicts bias behavior. These findings might also illustrate general mechanisms of past–present influences in neural operations.

Introduction

Although the outside world is changing constantly, natural stimuli maintain regularities over time [1,2]. Accordingly, perception is not solely determined by current sensory inputs, but largely shaped by past experiences, reflecting the exploitation of temporal regularities in the environment [3]. One striking example is serial dependence, that is, perception tends to be involuntarily biased towards stimuli in previous trials [4–8]. It has been robustly observed in a wide range of visual features, from simple ones like orientation [4,9–12], numerosity [13], and position [14,15] to abstract ones such as

China (https://www.nsfc.gov.cn, T2421004 to F.F. and H.L.), the National Science and Technology Innovation 2030 Major Program (https://www.most.gov.cn, 2021ZD0204103 to H.L.), National Natural Science Foundation of China (https://www.nsfc.gov.cn, 31930052 to H.L.), China Postdoctoral Science Foundation (https://www.chinapostdoctor.org.cn/bshjjh, 2020M680166 to H.Z.), National Science and Technology Innovation 2030 Major Program (https://www.most.gov.cn, 2022ZD0204802 to F.F.), National Natural Science Foundation of China (https://www.nsfc.gov.cn, 31930053 to F.F.). H.Z. was supported in part by the Postdoctoral Fellowship of Peking-Tsinghua Center for Life Sciences (https://cls.tsinghua.edu.cn). The funders played no role in the study design, data collection and analysis, decision to publish, or preparation of the manuscript.

Competing interests: I have read the journal's policy and the authors of this manuscript have the following competing interests: H.L. is a member of PLOS Biology's editorial board.

Abbreviations: AIC, Akaike information criterion; BEM, boundary element method; EOGs, electrooculograms; EEG, electroencephalography; ICA, independent component analysis; LCMV, linear constrained minimum variance; LMMs, linear mixed-effects models; MEG, magnetoencephalography; PFC, prefrontal cortex; PPC, posterior parietal cortex; RDM, representational dissimilarity matrix; RSA, representational similarity analysis; RT, reaction time; tSSS, spatiotemporal signal space separation; TMS, transcranial magnetic stimulation; WM, working memory.

facial attractiveness [16] and other modalities [17,18]. Despite its detrimental effects on perceptual fidelity, serial dependence is thought to reflect an optimizing strategy of the brain to increase perceptual stability and efficiency by taking advantage of inherent temporal correlations in a world that is presumably stable over a short time scale [19–21].

Two major theories have been proposed to account for the occurring stage of serial dependence. The "continuity field" view posits that serial dependence occurs at the perceptual level whereby similar stimuli of spatiotemporal adjacency are automatically integrated, leading to the widely observed attractive serial bias [4]. In contrast, the post-perceptual view [11,22] postulates a two-stage process consisting of perceptual-level efficient coding and post-perceptual Bayesian inference, associated with repulsive and attractive serial bias, respectively. Although large amounts of behavioral experiments have been performed to address the issue [9–11,23,24], neural evidence is certainly crucial to reconciling the arguments, which however remain mixed. For example, neural activities in visual cortex are shifted toward previous trials, advocating the perceptual "continuity field" view [25], while other studies reveal repulsive neural bias despite attractive bias behavior [26,27]. Animal electrophysiological studies and human Transcranial Magnetic Stimulation (TMS) studies demonstrate the involvement of higher-level regions, such as the prefrontal cortex (PFC) and posterior parietal cortex (PPC), in attractive serial dependence [28–30], thus advocating the post-perceptual view. It remains unclear how serial dependence dynamically emerges along various stages of processing and ultimately contributes to bias behavior.

In essence, serial dependence reflects the influence of past-trial memory trace on current information processing. PFC recordings on monkeys show that past information is transiently reactivated just before trial onset and correlates with bias behavior [28]. Our recent study [18] as well as previous works [31–34] demonstrate that past-trial features, retained in activity-silent states, are triggered by corresponding events within the current trial, and the co-occurrence of past and present contributes to serial bias [18]. However, past memory reactivation alone cannot explain serial bias, as the process must encompass interactions between past-trial reactivation and current-trial processing, presumably across multiple stages in different ways. Recent theoretical and empirical work reveals that the brain simultaneously represents distinct information in orthogonal neural subspaces to avoid mutual interference [35–39]. Accordingly, we hypothesize that for serial dependence to occur, past reactivations and present information need to reside in non-orthogonal subspaces, allowing them to interact, with aligned and flipped relationships giving rise to attractive and repulsive serial bias, respectively [26,33]. Thus, elucidating past-trial reactivations and past–present interactions across multiple brain regions is crucial for understanding the neural implementations of serial dependence.

The present study aims to unravel when, where and how serial dependence occurs by systematically examining past-trial reactivation and its interaction with present information processing in the whole brain using time-resolved measurements. Crucially, we developed a delayed-response task to explicitly separate

perception and decision-making stages so that their intertwined roles could be disambiguated and their involvements in serial dependence examined. Moreover, we dissociated stimuli and reports to examine what kind of past information affects present perception and decision-making. Behaviorally, participants showed attractive serial bias towards previously reported locations in continuous 2-D spatial perception. EEG/MEG recordings in two experiments demonstrate that the past-trial report information is reactivated and interacts with present information processing during both encoding and decision-making stages but in distinct ways, i.e., repulsive and automatic during encoding, while attractive, modulated by task relevance and correlated with behavior during decision-making, originated in the visual cortex and prefrontal cortex, respectively. Taken together, serial dependence arises from a two-stage past reactivation and "repulsive-followed-by-attractive" past–present interaction process, which might contribute to a wide range of themes beyond perception.

Results

Attractive serial dependence in 2-D continuous spatial perception

In Experiment 1, 29 human participants performed a delayed-response spatial location reproduction task with their 64-channel EEG activities recorded (Fig 1A). Specifically, a red dot was presented within a 2-D round area (Encoding stage) followed by a square noise mask, and participants reproduced the target location using a mouse starting at a random location (Decision-making stage). A multiple linear regression analysis (Fig 1B) revealed that the 2-D spatial reproduction performance ("Current Report") was modulated by stimulus location ("Current Stimulus"; mean = 0.92, 95% CI = [0.90, 0.94], $t(28) = 84.77$, $p < 0.001$, Cohen's $d = 15.7$), starting location of the mouse ("Current Start"; mean = 0.0080, 95% CI = [0.0044, 0.012], $t(28) = 4.56$, $p < 0.001$, Cohen's $d = 0.85$), and most importantly, the reported location in the preceding trial ("Previous Report"; mean = 0.0039, 95% CI = [0.001, 0.0069], $t(28) = 2.78$, $p = 0.0096$, Cohen's $d = 0.52$), indicating an attractive serial bias in behavior, i.e., the reported location was biased towards that of the previous trial.

Two-stage reactivations of previous-trial information

As serial dependence engages automatic past-to-present modulation, past information should be carried over and coexist with the current stimulus in the present trial. We therefore first sought to decode the stimulus location of preceding trial (N-1) and current trial (N) from the current-trial brain activities, by conducting a trial-wise representational similarity analysis (RSA) at each time point and on each participant (Fig 2A). Specifically, the dissimilarity (distance) of target locations within 2-D continuous space was calculated for each trial pair, based on which the representational dissimilarity matrix (RDM) was constructed (Location RDM). The neural dissimilarity matrix (Neural RDM) based on multivariate EEG patterns was then regressed by Location RDM, resulting in representational strength (Fig 2A, right). Notably, the RSA analysis was performed for current-trial and previous-trial location RDMs separately, resulting in the corresponding neural decoding time courses (Fig 2B, right).

First, as shown in Fig 2B (upper-right panel), information about current-trial target location emerged rapidly during encoding (20–520 ms after stimulus onset) and also appeared during the delay (0–320 ms, 360–490 ms after mask onset) and decision-making stages (60–760 ms after mouse cursor onset; cluster-based permutation test, $p < 0.05$, two-tailed, corrected). Crucially, previous-trial information (i.e., reported location in the previous trial) could also be decoded from the current-trial neural activities (Fig 2B, lower-right panel), reactivated during both encoding and decision-making stages (Encoding: 120–260 ms after stimulus onset; Decision-making: 230–300 ms and 330–410 ms after mouse cursor onset). Note that significant clusters in time courses were defined using the same statistical test and criteria unless otherwise specified (cluster-based permutation test, $p < 0.05$, two-tailed, corrected).

Therefore, previous-trial location information is indeed carried over to the current trial, and the memory reactivations co-occur with current stimulus processing during both the encoding and decision-making stages.

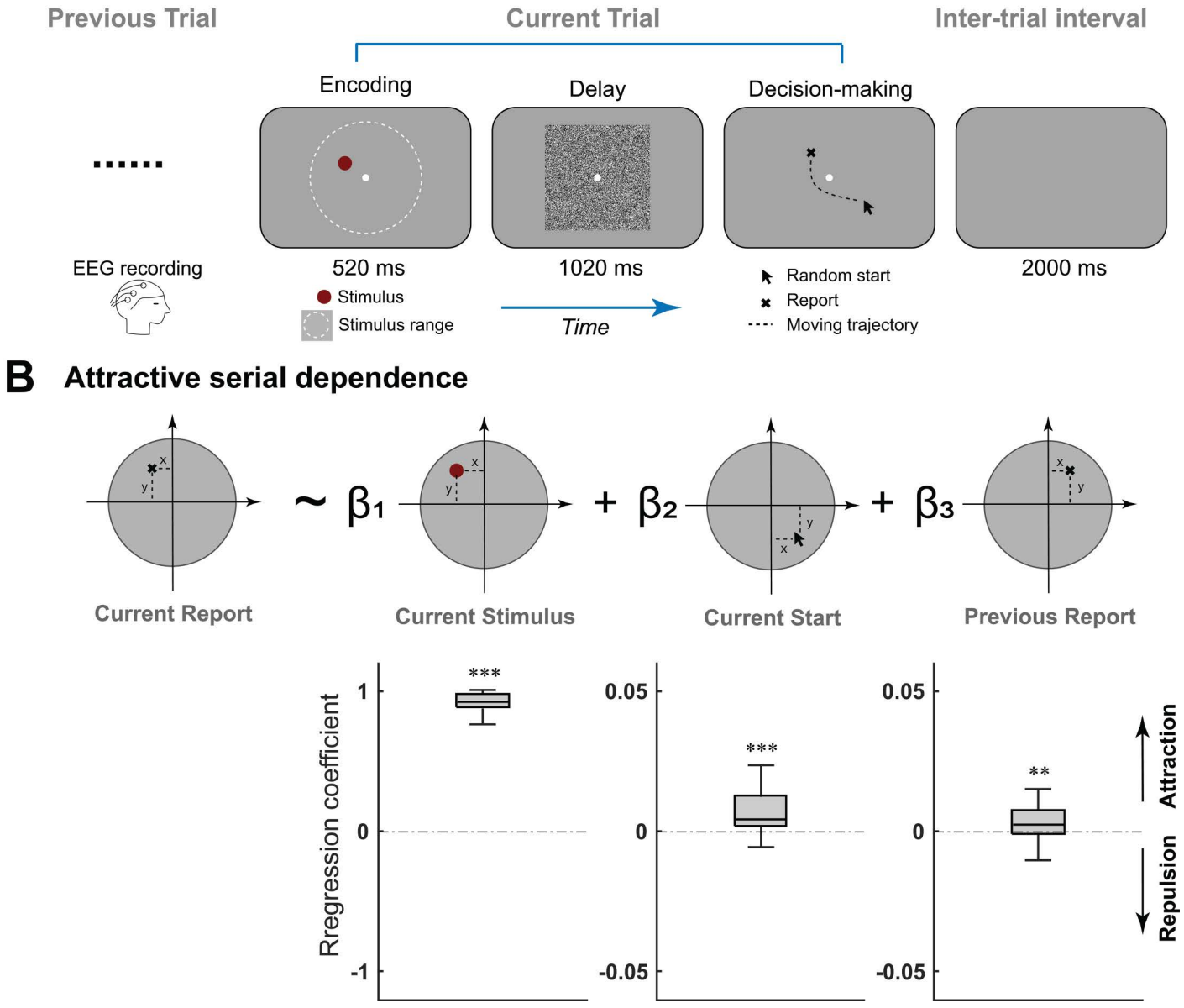

Fig 1. Attractive serial bias behavior in 2-D spatial perception task (Experiment 1, EEG). (A). On each trial, a red dot was randomly presented within a 2-D round area (Encoding period), followed by a square noise mask (Delay period). During Decision-making period, participants moved the mouse starting at a random location (Random start) to reproduce the red dot location, with their EEG activities recorded. **(B)**. Upper: a trial-wise linear regression model accounting for the reproduced location based on 3 factors: location of current target (current stimulus), starting location of mouse cursor (Current Start), reproduced location in previous trial (Previous Report). Lower: box plots of the regression coefficients (left to right: Current stimulus, Current Start, Previous Report). Edges from bottom to top indicate 25th, 50th and 75th percentiles, respectively. (**$p < 0.01$, and ***$p < 0.001$). Data supporting this figure can be found at: https://osf.io/c7dwp/.

https://doi.org/10.1371/journal.pbio.3003150.g001

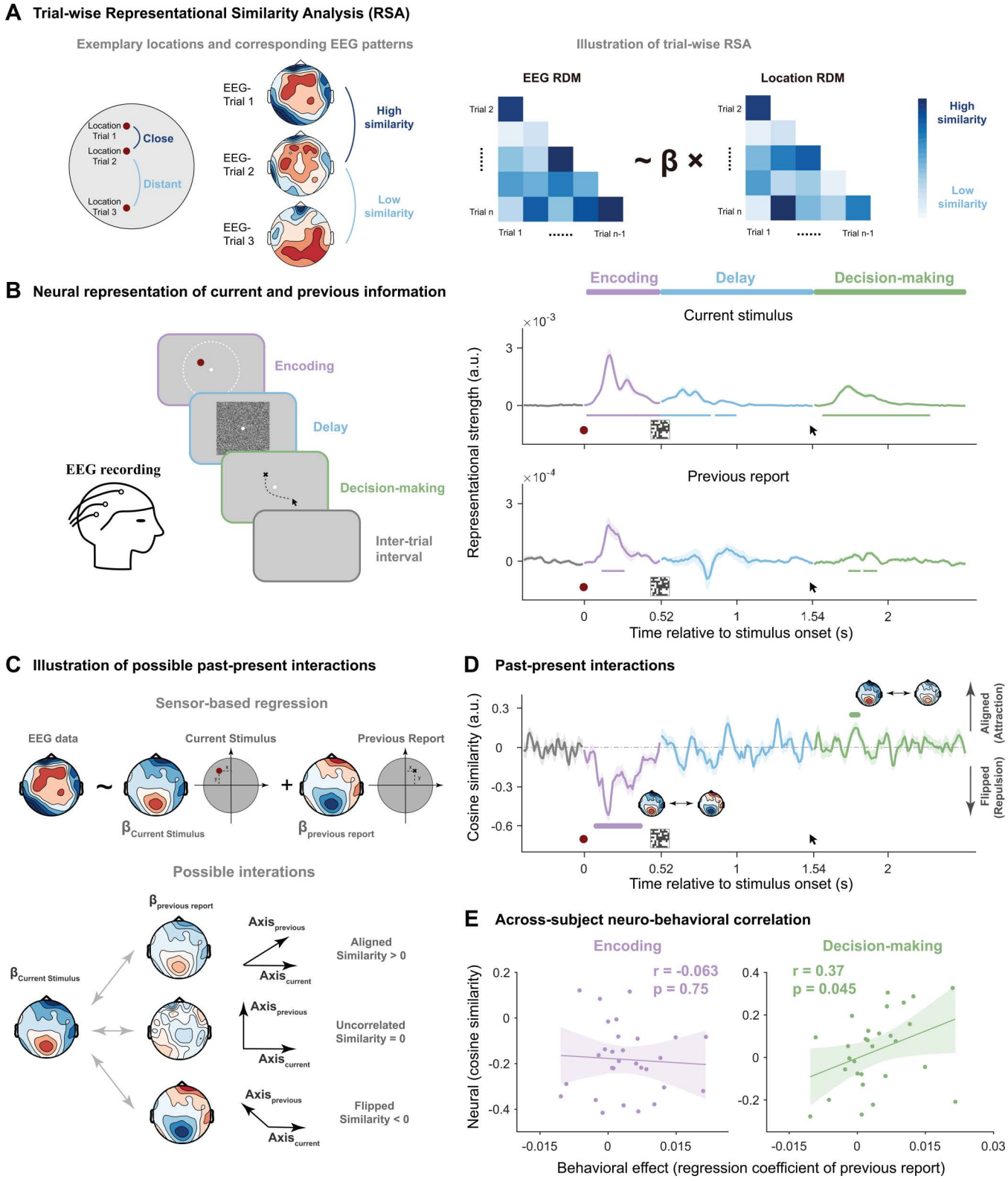

Fig 2. Neural decoding of current-trial and past-trial information, past–present neural interaction and its correlates to behavior (Experiment 1). **(A)**. Schematic illustration of trial-wise RSA (representational similarity analysis). Left: For every pair of trials, closer distance in dot location (dark blue)

is hypothesized to have more similar multivariate EEG pattern than that with far spatial distance (light blue), yielding the location RDM (right panel). Right: EEG RDM is calculated based on the multivariate EEG similarity for each pair of trials. Regression of EEG RDM into location RDM yields the regression coefficient (β) denoting the neural representation strength of location information. **(B)**. Left: Each trial consists of three stages: Encoding (purple), Delay (blue), and Decision-making (green). Right: Time-resolved grand averaged decoding of current-trial stimulus (upper) and past-trial reported location (lower). Note that the three stages – Encoding (purple), Delay (blue), and Decision-making (green) – start with onset of red dot, mask and arrow, respectively. **(C)**. Illustration of past–present neural interaction calculation. Upper: EEG data at each electrode (left topo) is first regressed to current stimulus and previous report, yielding respective weight maps ($\beta_{Current\ Stimulus}$, $\beta_{Previous\ Report}$). Lower: Each weight map could be denoted as a vector in the 64-dimensional representational space. Past–present interactions are quantified by computing cosine similarity between the vector for current stimulus and the vector for previous report. Positive, zero, and negative values represent aligned, uncorrelated, and flipped relationship, respectively. **(D)**. Time-resolved grand averaged past–present interactions throughout Encoding (purple), Delay (blue) and Decision-making (green) stages. **(E)**. Cross-subject correlation between serial dependence behavior (*x*-axis; regression weight) and past–present neural interaction (*y*-axis; averaged within significant clusters) during Encoding (left, purple) and Decision-making (right, green) stages. Each dot denotes individual subject. Solid lines denote the best linear fitting. Shaded areas denote 95% confidence interval. For all time-resolved plots, solid lines denote grand average. Shaded areas denote ±1 SEM. Horizontal lines denote significant temporal clusters (cluster-based permutation test, $p < 0.05$, two-sided, corrected). Data supporting this figure can be found at: https://osf.io/c7dwp/.

https://doi.org/10.1371/journal.pbio.3003150.g002

Two-stage "repulsive-followed-by-attractive" past–present interactions and behavioral correlates

After confirming the co-occurrence of past and present information, we next examined their interaction during both encoding and decision-making stages, focusing particularly on shifting directions, i.e., attractive or repulsive. Given previous theoretical and empirical animal studies showing that non-orthogonal sensory and memory representational axes could lead to interference [35,36,38], we directly estimated the representational axes for past and present and examined their angular relationship (see section "Methods" for details). Specifically, we examined the neural similarity in representations between past memory reactivation and current stimulus, with positive and negative values denoting attractive (aligned) and repulsive (flipped) bias, respectively (Fig 2C, lower). To this end, the neural signal of each EEG channel was regressed by three predictors (Current Stimulus, Current Start, Previous report; see Fig 1B), resulting in a 64-dimensional EEG topographic map of regression coefficients (neural representational axis) for each predictor (Fig 2C, upper). Next, the cosine similarity between the 64-dimensional representational axis of Previous Report and that of Current Stimulus was computed, signifying the past–present interaction (Fig 2C, lower). The sign of the past–present interaction value denotes three possible bias directions – aligned (positive value), flipped (negative value), and uncorrelated (near to zero) – corresponding to attractive, repulsive, and non-interactions, respectively (Fig 2C, lower). This analysis was performed at each time point and on each participant.

As shown in Fig 2D, the past–present interactions exhibited a two-stage dissociated profile: repulsive interactions during encoding (80−370 ms after stimulus onset) and attractive interactions during decision-making (250−290 ms after mouse cursor onset). Furthermore, we examined the behavioral relevance of the two-stage past–present neural interactions, by calculating the Pearson's correlation coefficients between serial bias behavior ($\beta_{Previous\ Report}$, see Fig 1B) and past–present neural interactions (i.e., averaged within significant temporal clusters, see Fig 2D) across participants, for encoding and decision-making periods, separately. As shown in Fig 2E, only the late attractive interactions correlated with the attractive bias behavior ($r(28) = 0.37$, $p = 0.045$), but not for the early repulsive interactions ($r(28) = -0.063$, $p = 0.75$). Overall, although past-trial information is reactivated during both encoding and decision-making stages, it interacts with present information processing in an opposite two-stage manner: repulsive (flipped) during sensory encoding and attractive (aligned) during decision-making, with the latter further related to attractive serial dependence behavior.

Past choice instead of past stimulus mediates attractive serial bias

In Experiment 1, stimulus (target location) and report (reproduced location) were highly correlated, making it hard to disentangle the contributions of previous stimulus and previous report to serial bias. Furthermore, it remains unclear how task relevance impacts the observed two-stage process and the underlying brain regions. In Experiment 2, we employed a modified paradigm with MEG recordings to address these questions.

As shown in Fig 3A, participants were presented with two dot stimuli of different colors at two random locations. During decision-making, they recalled the location of one of the two dots based on the retrocue color (Target versus Non-target dot stimuli), by choosing from two of the response probes closest to the cued target location (Chosen versus Unchosen response probe) (Fig 3A, right). Critically, this design could dissociate stimulus and report, since the dot stimuli (Target) and response probes (Chosen) were localized at different locations. Moreover, task-relevance could also be studied based on Chosen versus Unchosen and Target versus Nontarget. Twenty-six subjects participated in Experiment 2 and performed well (Fig 3B; report accuracy: 0.90 ±± 0.033; reaction time: 1.77 ± ± 0.57). Due to high accuracy rates across trials, which may limit the sensitivity to detect serial dependence effects, we converted the binary probe choice into a continuous scale (−1 to 1) by incorporating reaction time (RT) as a weighting factor (see Methods for details) to better capture behavioral patterns. This rationale for using RT to index the serial dependence effect is based on previous findings that past choices can enhance the evidence accumulation rate during decision-making and accelerate response times [20,40].

First, Linear mixed-effects models (LMMs) with various combinations of factors (Current target, Current non-target, Previous target, Previous non-target, Previous chosen, Previous unchosen) were built to evaluate their contributions to behavior (Fig 3C). Specifically, candidate models were built in a stepwise manner (gradually adding factors) and compared to the base model (i.e., Current target only), yielding their respective Akaike information criterion (AIC) values with lower value indicating better performance. As shown in Fig 3C (lower panel, star), the model comprising Current target, Current non-target, Previous chosen, and Previous unchosen factors performed best (ΔAIC = −35.57; see S1 Table for model comparison details), suggesting that current choice is biased by past-trial choice (chosen and unchosen) rather than past-trial stimuli (target and non-target). Moreover, regression coefficients extracted from each subject reveal different directions of the four factors biasing the current choice, with positive values (attractive) for Current target and Previous chosen and negative values (repulsive) for Current non-target and Previous unchosen (Fig 3D; Current target: 0.13 ± 0.016, $t(25) = 42.80$, $p < 0.001$, Cohen's $d = 8.39$; Current non-target: −0.0052 ± ± 0.0092, $t(25) = -2.91$, $p = 0.0075$, Cohen's $d = 0.57$; Previous chosen: 0.0039 ± ± 0.0082, t(25) = 2.43, $p = 0.023$, Cohen's $d = 0.48$; Previous unchosen: −0.0038 ± ± 0.0055, $t(25) = -3.53$, $p = 0.0016$, Cohen's $d = 0.69$; one-sample t test, two-tailed).

In summary, by employing a modified paradigm in Experiment 2 to separate stimulus and choice information, we demonstrate that the typical attractive serial dependence arises primarily from past-trial choice rather than past-trial stimulus. Moreover, task relevance also modulates serial bias.

Two-stage reactivations of past choice

We used the same trial-wise RSA decoding method as Experiment 1 to decode variables that essentially contribute to serial dependence (i.e., the best model in Fig 3C) from MEG activities. As shown in Fig 4A (right), consistent with Experiment 1, target location (Current target) emerged during encoding (0–500 ms after stimulus onset), delay (0–610 ms after mask onset), recalling and decision-making stages (0–500 ms after retro-cue onset; 0–1,000 ms after probe onset). Interestingly, although the uncued stimulus (Current non-target) could be discarded after the retrocue, the non-target still emerged during recalling and decision-making (0–140 ms 185–500 ms after retro-cue onset; 0–235 ms 280–1,000 ms after probe onset). Thus, current-trial stimulus information is maintained throughout the trial, regardless of task relevance.

In contrast, previous-trial choice reactivations are modulated by task relevancy. Specifically, although the past-trial choice (Previous chosen) was reactivated during encoding (150–500 ms after stimulus onset), delay (140–310 ms after mask onset), and decision-making stages (320–405 ms, 620–765 ms after probe onset), the past-trial unchosen probe (Previous unchosen) was only reactivated during early encoding (270–420 ms after stimulus onset) but not during the late decision-making stage.

Therefore, past-trial reactivation also exhibits a two-stage profile. Both previous chosen and unchosen information is reactivated during early encoding, but only the previous choice is conveyed to the late decision-making stage.

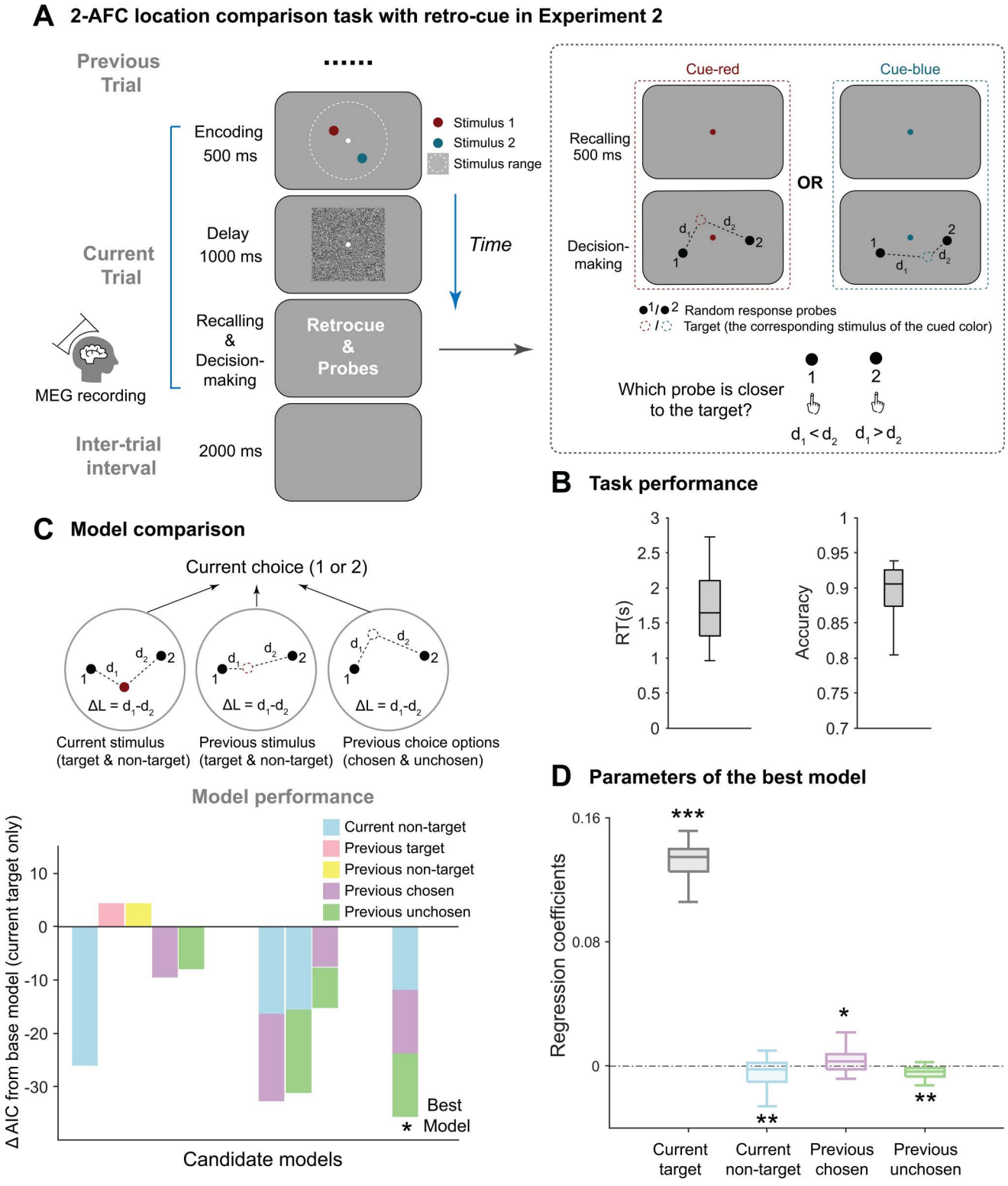

Fig 3. Experimental paradigm and behavioral serial biases (Experiment 2, MEG). (A) Participants were presented with two colored dots with random location within a 2-D round area, followed by a square mask in the delay period. Afterward (dotted box in the right), a retro-cue (changing color of central fixation) indicated which dot need to be recalled (target versus non-target). During decision-making, two randomly located response probes

(marked by 1 and 2) were presented and participants selected the one closest to the target location. Subjects' MEG activities were recorded. **(B)**. Grand averaged accuracy and reaction time (RT). **(C)**. Model comparison results. Upper: Factors considered to contribute to current-trial choice. Six locations are divided into three categories: current stimulus (target and non-target), previous stimulus (target and non-target) and previous choice option (chosen and unchosen). Lower: ΔAIC of candidate models compared against the base model (current target only). The best model (with the lowest AIC) among all candidates is indicated with an asterisk. Key factors of candidate models are color-coded. **(D)**. Regression coefficients extracted from the best model. For all the box plots, the bottom edge, central mark and top edge denote the 25th, 50th and 75th percentiles, respectively, and the whiskers extend to the most extreme data points not considered outliers. (***$p < 0.001$, **$p < 0.01$, *$p < 0.05$). See also S1 Table. Data supporting this figure can be found at: https://osf.io/c7dwp/.

https://doi.org/10.1371/journal.pbio.3003150.g003

Task relevance modulates two-stage past–present interactions and their behavioral correlates

Experiment 1 revealed two-stage past–present interaction and its relevance to bias behavior. We used the same approach to calculate neural similarities between past-trial choice and current-trial target/non-target, denoting past–present neural interactions under task-relevant and task-irrelevant conditions, respectively. Similar to Experiment 1, positive and negative values indicate attractive (aligned) and repulsive (flipped) bias (Fig 4B). As shown in Fig 4C, the early encoding stage (in purple) displayed repulsive past–present interaction for both target (upper; 170–255 ms, 315–385 ms, 405–460 ms) and non-target (lower; 170–265 ms, 290–395 ms, and 415–490 ms after stimulus onset). Meanwhile, during late decision-making (in dark-green), past choice only interacted with current target in an attractive direction (upper; 230–400 ms after probe onset), but not with non-target (lower panel, see S1 Fig for repulsive interaction between past unchosen and current target during encoding).

We next examined the behavioral relevance of past–present interactions. Motivated by previous studies positing that one benefit of attractive serial bias is to speed up perception and decision-making processes [20,40], we used trial-wise reaction time (RT) to quantify serial bias behavior and computed correlations between the inverse of RT (behavioral index) and trial-wise neural interactions (neural index, see details in "Methods" section) within each participant (see S2 Fig for other across-participant correlation results). As shown in Fig 4D, only the late attractive past–present neural interaction correlates with serial bias behavior ($\beta = 5.02 \times 10^{-4} \pm 9.62 \times 10^{-4}$, $t(25) = 2.66$, p = 0.014, Cohen's $d = 0.52$, one-sample *t* test, two-tailed), while the early repulsive interaction did not ($\beta = 8.38 \times 10^{-5} \pm 7.19 \times 10^{-4}$, $t(25) = 0.59$, p = 0.56, Cohen's $d = 0.12$, one-sample *t* test, two-tailed).

Overall, Experiment 2 confirms the two-stage "repulsive-then-attractive" past–present interactions found in Experiment 1 (Fig 2D), and further demonstrates the dissociated nature of sensory-encoding and decision-making stages: the early stage is automatic and adaptation-like, and the late stage tends to be modulated by task demands and essentially contributes to typical attractive serial bias behavior.

Two-stage past–present interactions arise in dissociated brain regions

MEG activities were recorded in Experiment 2 to examine spatiotemporal neural dynamics of past–present interactions. We finally investigated brain regions associated with the two-stage past–present interactions. We first addressed the question at sensor levels (Fig 5A and 5B), by dividing all the MEG sensors into anterior (green) and posterior (purple) ones, and performed the same analyses on the two halves separately. First, the posterior regions (purple) dominated the early encoding stage (Fig 5A), exhibiting reactivation of previous choice (150–370 ms, 405–495 ms) as well as repulsive past–present interaction (175–275 ms, 310–390 ms). Meanwhile, the anterior regions (green) drive the late decision-making stage (Fig 5B), with significant past reactivation (110–410 ms, 605–755 ms) and positive past–present interaction (365–510 ms, 540–635 ms).

We next examined the source level, by performing the same analyses within each of 34 surface regions of Desikan–Killiany Atlas [41]. Consistent with sensor-level results, brain regions mediating past–present interaction during encoding (Fig 5C, dark purple) were located in posterior areas (cluster-based permutation, $p < 0.05$, two-tailed, spatial-temporally corrected). Specifically, regions showing significant past reactivations included the lateral occipital cortex, cuneus,

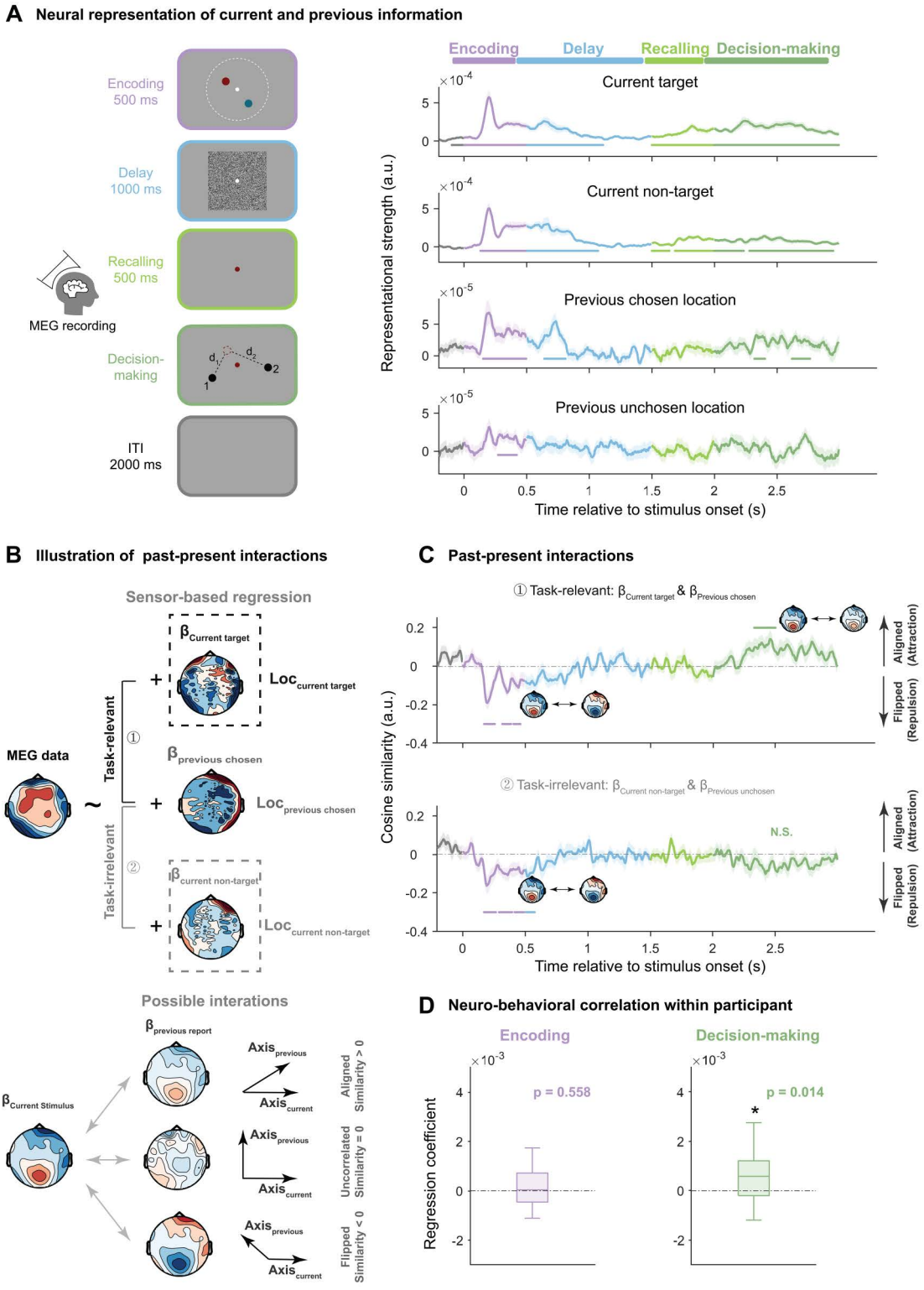

Fig 4. Neural decoding and past–present interactions in Experiment 2 (MEG). (A) Left: Each trial consists of four stages: Encoding (purple), Delay (blue), Recalling (light green), and Decision-making (dark green). Right: Time-resolved grand averaged decoding of current-trial stimulus (target and non-target dot stimuli) and previous-trial choice (chosen and unchosen response probes). **(B)** Same past–present neural interaction computation as

in Experiment 1 (see Fig 2) was performed in Experiment 2 on MEG sensors. Upper panel: past–present interaction was calculated between weight map of current stimulus (Upper: task-relevant target; Lower: task-irrelevant non-target) and that of previous chosen location (middle), resulting in task-relevant and task-irrelevant past–present neural interactions. Lower panel: three possible interaction directions, with positive, zero, and negative values representing aligned, uncorrelated, and flipped relationship, respectively. **(C)** Time-resolved grand averaged past–present neural interaction under task-relevant (between previous choice and current target) and task-irrelevant (between previous choice and current non-target) conditions. The shaded areas denote ±1 SEM. Positive and negative values represent aligned and flipped directions, respectively. **(D)** Within-participant correlation between behavioral effect (RT benefit) and past–present neural interaction (averaged within significant clusters) cross trials during encoding (left, purple) and decision-making (right, green) stages, with bottom edge, central mark and top edge denoting the 25th, 50th and 75th percentiles, respectively. The whiskers extend to the most extreme data points not considered outliers. *$p < 0.05$. For all time-resolved plots, solid lines denote grand average. Shaded areas denote ±1 SEM. Horizontal lines denote significant temporal clusters (cluster-based permutation test, $p < 0.05$, two-sided, corrected). See also S1 and S2 Figs. Data supporting this figure can be found at: https://osf.io/c7dwp/.

https://doi.org/10.1371/journal.pbio.3003150.g004

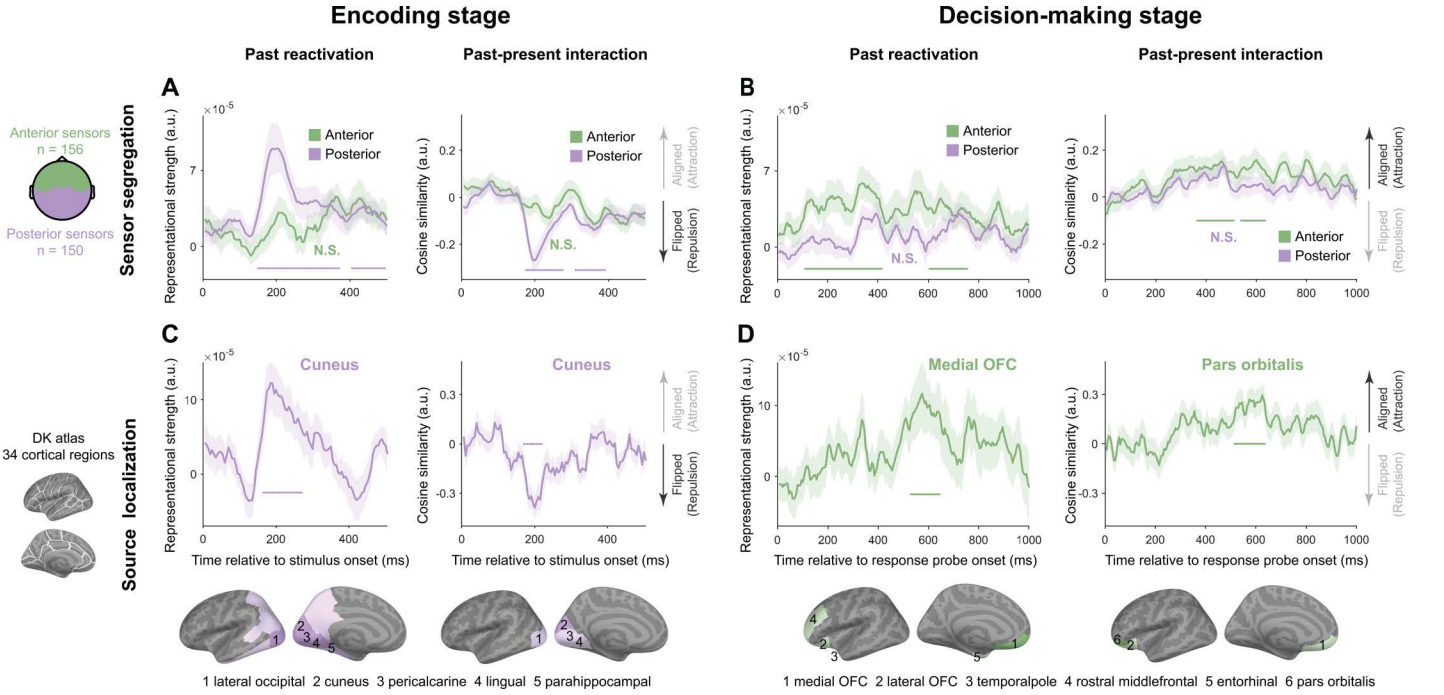

Fig 5. Two-stage cortical origins of serial biases (Experiment 2, MEG). (A–B) Sensor-based results. 306 MEG sensors are split into 156 anterior (green) and 150 posterior (purple) halves (leftmost, up), within which analyses are performed separately. **(A)** Sensor-level results during Encoding stage. Time-resolved grand averaged decoding of previous chosen location information (left) and past–present neural interactions (right), for anterior (green) and posterior (purple) halves. Positive and negative values in past–present interaction represent aligned and flipped directions. **(B)** The same as **A** but during Decoding-making state. (**C–D)** source-level results. Analyses are performed for each of the 34 cortical regions identified based on the Desikan–Killiany atlas (leftmost, bottom) separately. **(C)** Source-level results during Encoding stage. Upper: Time-resolved grand averaged decoding of previous chosen location information (left) and past–present neural interactions (Right) within cuneus, a representative sensory region. Lower: Significant regions during Encoding stage displayed on inflated cortical surface with their names shown at bottom. Dark and light colors denote temporal clusters with or without spatial corrections. **(D)** Same as **C** but during Decision-making stage. Upper: Time courses within PFC regions (Medial OFC for past reactivation, left; Pars Orbitals for past–present interaction, right). Shaded areas denote ±1 SEM. Color-coded horizontal lines denote corresponding significant clusters (cluster-based permutation test, $p < 0.05$, two-tailed, corrected). N.S. denotes nonsignificant. See also S3 Fig. Data supporting this figure can be found at: https://osf.io/c7dwp/.

https://doi.org/10.1371/journal.pbio.3003150.g005

peri-calcarine, lingual and parahippocampal areas (Fig 5C, left, dark blue), and past–present interaction occurred in the cuneus region (Fig 5C, right, dark blue). In contrast, during late decision-making, anterior brain regions played major roles (Fig 5D, dark green; cluster-based permutation, $p < 0.05$, two-tailed, spatio-temporally corrected), with reactivation of previous choice in the medial orbitofrontal cortex (medial OFC; left, dark green), and the past–present interaction in pars

orbitalis (right, dark green). Note that light colors denote significant regions without spatial corrections. Importantly, the grand average time course within the corresponding source-level regions displayed temporal profiles commensurate with sensor-level results (Fig 5C and 5D, upper; see S3 Fig for time courses in other regions).

Taken together, the two-stage "repulsive-followed-by-attractive" past–present interactions are mediated by dissociated brain regions, i.e., early visual cortex and prefrontal cortex, respectively.

Discussion

Serial dependence, as a robust and automatic effect occurring on a wide range of features and paradigms, reflects a general past-to-present influence of neural processing. Here, across two experiments with EEG/MEG recordings, we unveil a unifying framework for its complex operation (see illustration in Fig 6). First, the goal-based report, instead of the stimulus

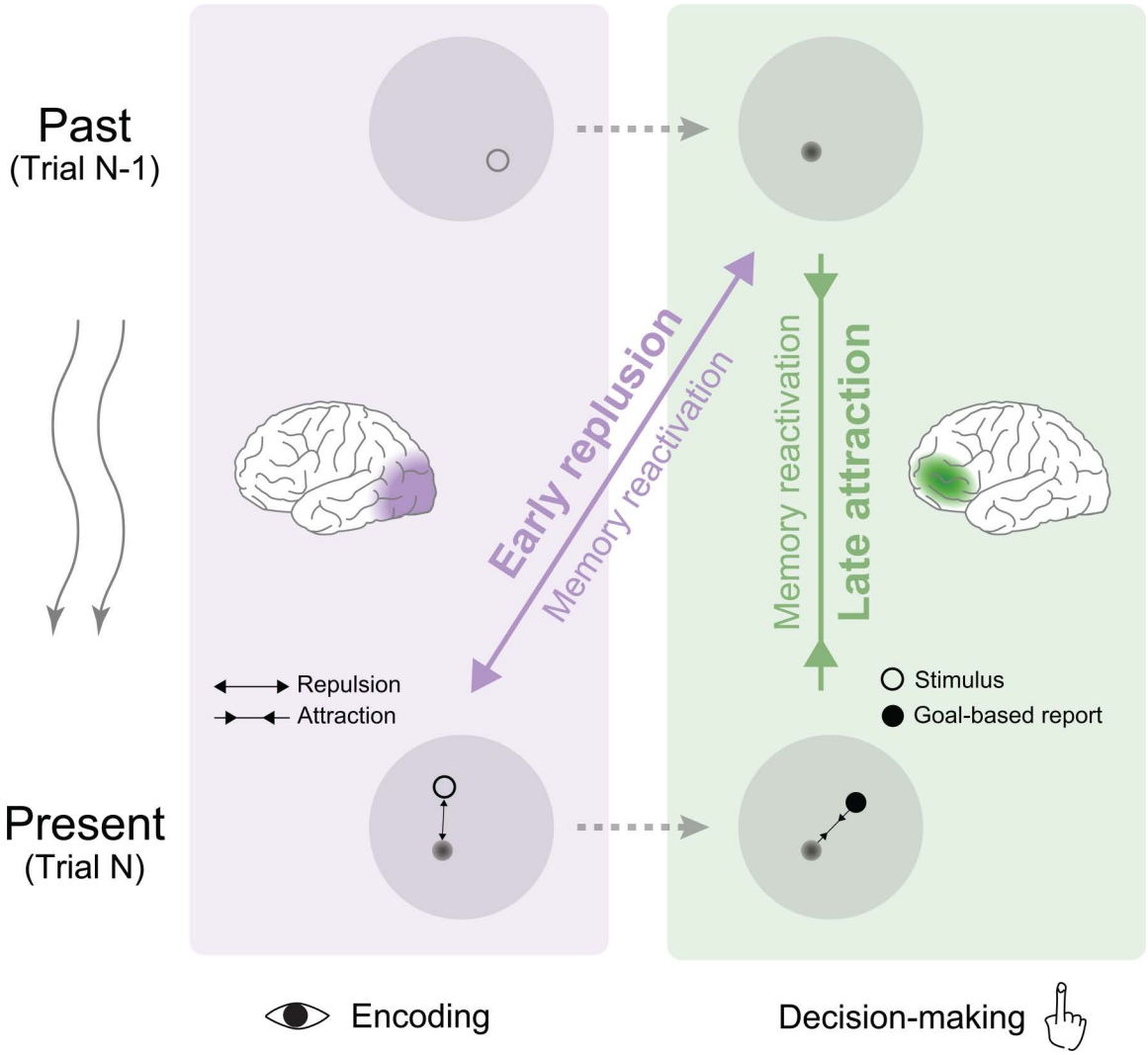

Fig 6. A two-stage operational mechanism for serial dependence. The past-trial goal-based report (upper panel), stored in distinct mnemonic formats in the sensory (purple box) and prefrontal cortex (green box) (middle panel), is reactivated during present-trial information processing (lower panel). The past–present interactions occur in two stages: early repulsion and late attraction. The brain icons are drawn using codes from Scholtens, L. H., de Lange, S. C., and van den Heuvel, M. P. (2021). Simple brain plot (v1.0.0). Zenodo. https://doi.org/10.5281/zenodo.5346593.

https://doi.org/10.1371/journal.pbio.3003150.g006

itself, exerts influence on incoming information processing. Second, past reports are stored in distinct memory formats—either sensory-like or abstract—and are reactivated during both sensory encoding and decision-making stages. Notably, past reactivation interacts with current information processing in two distinct ways: initially repelling the present during encoding and later attracting it during decision-making, originating from the sensory cortex and prefrontal cortex, respectively. While the early interaction occurs automatically, the late stage is modulated by task relevance and predicts serial bias. The two-stage past–present interplay might also illustrate the general mechanisms of past-to-present influences in many cognitive functions.

A key finding here is the non-orthogonal representations of present information and memory reactivations underlying serial dependence. Theoretical models suggest that working memory (WM) retains multiple items in near-orthogonal neural subspaces to minimize mutual interference [35,36], a concept supported by recent empirical studies. For instance, prefrontal cortex (PFC) recordings in monkeys indicate that rank information in a sequence is encoded in orthogonal neural subspaces [37]. Similarly, Libby and Buschman (2021) demonstrate that the auditory cortex rotates memory representations to be orthogonal to incoming sensory inputs, reducing sensory-memory interference [38]. Moreover, human PFC has been shown to resolve cognitive interference by partitioning past and present states into non-overlapping subspaces [39]. In line with these theoretical and empirical insights, we find that past reactivations and present representations reside in non-orthogonal subspaces to interact. To further validate our neural interaction findings, we conducted an additional analysis by decoding present location using a linear decoder and examining the influence of past reports. The results reveal that past reports negatively predict reconstructed locations during encoding but positively predict them during decision-making (S5 Fig). Together, these findings suggest that neural biases can be quantified by the neural alignment of past reactivations and present information in either a repulsive or attractive direction.

It has been extensively debated at which stage serial dependence occurs [4,5,11,22,23]. Despite large amounts of behavioral studies, neural evidence remains mixed and scarce [25–27,42]. For example, John-Saaltink and colleagues found attractive bias in primary visual cortex, implying a low-level occurrence of serial dependence [25]. However, recent studies revealed automatic repulsive neural bias in sensory areas, but they did not discover late attractive neural bias and its brain origin [26,27]. Complementarily, other studies found the causal role of prefrontal cortex in the attractive serial dependence [28,30], in support of its post-perceptual origin. The mixed findings might be due to the rapid co-evolving information flows across brain regions that are difficult to disambiguate in previous paradigms. Here, within a single study, by temporally separating encoding and decision-making stages in delayed-response tasks and leveraging the good spatiotemporal resolution of MEG, we demonstrate the neural dynamic of past–present interactions across various cognitive stages and in distinct brain regions, being repulsive during sensory encoding and attractive during high-level decision-making, thus unifying previous contradictory findings and advocating the two-stage account of serial dependence [11,22].

The early repulsive past–present interaction reflects sensory adaptation that promotes novelty detection based on efficient coding principles [11,22,43]. Recent stimuli, either across-trial or within-trial, are found to repel present sensory processing, especially when stimuli are of high intensity and long duration [4,26]. Visual cortical recordings of rats reveal long-term stimulus-specific adaptations triggered by brief stimuli [44]. Here, the repulsive past–present interactions occur in the sensory cortex, thus consistent with previous findings [26,27,45]. Moreover, reactivations of both chosen and unchosen past-trial probes as well as their repulsive interactions with current stimulus in the sensory cortex, which further correlate with repulsive serial bias behavior (S2 Fig), also highlight the automatic nature of low-level efficient coding at the early stage of serial dependence. A recent study showed that adaptation is accounted for by early neural ‘fatigue’ and late neural ‘sharpening’, presumably reflecting distinct feedforward and feedback interactions [46]. The observed repulsive sensory bias here is in line with this ‘sharpening’ mechanism, wherein the reactivated past information might serve as feedback or local recurrent signals to ‘sharpen’ the present neural response, i.e., efficient coding.

The late attractive past–present interaction, in contrast, occurs during decision-making in the prefrontal cortex such as OFC and IFG. This is also in line with previous findings disclosing the involvement of higher-level areas (e.g., PPC and dlPFC) in attractive serial bias [28,29,47–49]. The two-stage model posits that attractive serial bias emerges from

post-perceptual Bayesian inference [10,11,22,24,27], through which prior information is integrated with current information in the prefrontal cortex [50–52]. In addition, task relevance modulates the attractive past–present neural interaction, similar to previous findings [26,53]. Furthermore, the reactivated past choice aligns with target in neural representations but is orthogonal to non-target (nonsignificant past–present interactions). This representational orthogonalization might help minimize interference from task-irrelevant distractors in Bayesian integration [35,39]. Finally, as past-trial choice is not reactivated by retrocue during WM retention but activated during decision-making to mediate attractive serial bias, our results also indicate that the post-perceptual attractive bias occurs during decision-making rather than WM maintenance, in line with a recent finding [54]. It seems inconsistent with another finding of an attractive neural bias during memory retrieval [55]. However, unlike our study, after the retro-cue in their cued reproduction task, participants already practically enter the "decision-making" stage, i.e., deciding which one to reproduce. Thus, if we refer decision-making as a direct goal-achieving process, the attractive serial dependence manifests in this stage in both cases.

Both repulsive and attractive past–present interactions rely on memory reactivations of past. Consistent with the 'activity-silent' WM theory [56], recent studies show that past-trial information silently stored in WM could be reactivated either before stimulus onset or after [18,28,31–34,57]. Here, past chosen and unchosen probes leading to opposite serial bias behaviors are reactivated differently, suggesting a substantial role of memory reactivation in serial dependence. Notably, our previous study revealed feature-specific characteristics of past reactivation, i.e., reactivated by corresponding features [18]. Meanwhile, since it is an instantaneous perceptual decision-making task where sensory encoding and decision-making co-evolve, the stages for these feature-specific reactivations could not be identified. Here, by using delayed-response tasks to separate encoding and decision-making stages within a trial, we show clear dissociated stages of past reactivations. Specifically, the failure of retrocue in reactivating past-trial information extends previous findings and suggests that past reactivation is not a fixed pattern but flexible and task-dependent. Specifically, the retrocue is limited to current stimuli, while the goal-based decision-making stage necessitates activations of past goal-related information (i.e., prior) and present decisional evidence. Finally, past information is retained in sensory and temporal-parietal regions during encoding and frontal-temporal regions during decision-making, supporting distributed neural substrates of WM [58], and different storage formats for memory, i.e., sensory or abstract representations [59–61]. Moreover, our findings cannot be attributed to eye movements, as both the encoding and decision-making stages—despite presumably involving similar eye movement profiles—exhibit past reactivations in distinct brain regions. Notably, the observed past reactivation in the mPFC aligns with previous decision-making literature, which highlights its role in encoding past and present hidden states [62].

To understand the whole loop of serial dependence, in addition to locating its operating stage, identifying the site of prior generation, i.e., where is the information that induces future biases constructed, is also crucial [5]. Converging evidence has shown that prior information causing attractive serial bias is a high-level construct, which is a subjective perception or decision that can incorporate context-information and requires conscious awareness [12,17,18,23,53,63]. However, stimuli and responses are highly correlated, making it challenging to distinguish whether the prior is based on pure report or stimulus. We demonstrated that it is previous reports rather than previous stimulus that contributes to serial bias. Hence, the prior causing attractive bias is a high-level conscious construct derived from task goals. Our findings could not arise from recency effects, since target stimulus that is consciously held in working memory is processed simultaneously with the response probe, yet only the chosen probe shows the attractive serial bias.

Taken together, combining EEG/MEG recordings with task paradigms that temporally differentiate cognitive stages and dissociate task variables, we demonstrate the operational circle of serial dependence. The goal-based report formed during decision-making constitutes the prior that biases subsequent perception and decision-making. Sensory traces and abstract codes, stored in different memory-related regions, are reactivated during incoming encoding and decision-making stages, and repulsively and attractively influence current information processing, respectively. This two-stage past–present influence illustrates how the brain balances novelty detection with stable perception over time and provides potential insights into other cognitive functions.

Methods

Ethics statement

In Experiment 1 (EEG study), we recruited 31 participants, and two were excluded from further analysis because one didn't finish the task, and one performed poorly (falling asleep during the task). For the remaining 29 participants (13 females), their age ranges from 18 to 27 (mean = 21.6, SD = 1.83). In Experiment 2 (MEG study), 27 participants were recruited and one was excluded from further analysis because of poor performance (accuracy lower than 3 standard deviations from the group mean). The age for the remaining 26 participants (17 females) ranges from 19 to 26 (mean = 21.6, SD = 2.02). All participants in the two experiments have normal or corrected-to-normal visions.

We obtained formal written consent from participants before they commenced the experiments. Both experiments were approved by the Ethics and Human and Animal Protection Committee (approval number: #2021-10-15), School of Psychological and Cognitive Sciences, Peking University, and were conducted in accordance with the Declaration of Helsinki.

Experimental design

Apparatus and materials. Both experimental programs were developed using Matlab (MathWorks Inc., 586 Natick, MA, USA) and Psychophysics Toolbox [64]. In Experiment 1 (EEG study), all visual stimuli were displayed on a 32-inch Display++ LCD screen with a refresh rate of 100 Hz and a resolution of 1,920 × 1,080 pixels. Participants sat 57 cm away from the screen and we used a chin-rest to keep their head steady. In Experiment 2 (MEG study), Visual stimuli were presented on a 26-inch rear-projection screen with a resolution of 1,024 × 768 pixels and a refresh rate of 60 Hz. The screen was 75 cm away from the participants. In both experiments, all the visual stimuli were presented on a gray background.

Experimental procedure in Experiment 1 (EEG study). Participants were instructed to reproduce the location of a red dot by moving and clicking a mouse (Fig 1A). Locations of the red dot and the mouse cursor's start point were independent, both randomly sampled from a uniform distribution within a 2-D round area (15° visual angle in diameter, edge indicated by the white dashed circle in Fig 1A). Specifically, in each trial, a red dot (0.4° visual angle in diameter) was first presented for 520 ms, and then masked by a square noise patch (white noise smoothed with a 0.91° standard deviation Gaussian kernel, 15° visual angle in diameter) for 1,020 ms, after which a mouse cursor appeared at a random location. Participants had to view and memorize the red dot's location while maintaining their fixation at a central white dot (0.2° visual angle in diameter) that was presented throughout the trial. After seeing the mouse cursor, they needed to move it to the remembered location of the red dot and left-click. They could adjust their response by moving and clicking it again. When they were satisfied with their response, they could press the 'space' key to submit their final report and end the trial. There was no time limit for the response. A blank screen with gray background was presented for 2000 ms before the next trial started. Participants first completed a practice session of 10 trials, and then started the formal experiment, which consisted of 32 blocks of 50 trials each, with a one-minute break between blocks. EEG activities were recorded throughout the experiment.

Experimental procedure in Experiment 2 (MEG study). Participants viewed and memorized two differently located and colored dots (red and blue) and recalled one of them to do a location comparison task (Fig 3A). In each trial, participants first viewed both red and blue dots, which were independently and randomly drawn from a uniform distribution within a 2-D round area (15° visual angle in diameter, edge indicated using white dashed circle in Fig 3A), for 500 ms (Encoding), and then encountered a mask of square noise patch (white noise smoothed with a 0.91° standard deviation Gaussian kernel, 15° visual angle in diameter) for 1,000 ms (Delay). During the encoding and delay stages, participants had to maintain their fixation on a central white dot (0.2° visual angle in diameter). In the next recalling stage, the color of the central fixation changed to either red or blue, indicating which item had to be extracted from memory and used in the following location comparison task. We referred to the retro-cued item as "target" and the uncued one as the "non-target".

Two black dots ("probe", labeled 1 or 2), which were also independently and randomly drawn from a uniform distribution within the same 2D round area as the red and blue dots, were presented on the screen 500 ms after the appearance of the retro-cue, and participants were asked to indicate, by keyboard input (choosing 1 or 2), which probe was closer to the location of the memorized "target". There was no time limit in their response. A blank screen with gray background was presented for 2000 ms before the next trial started. Each participant practiced 20 trials first, and those with at least 75% accuracy were allowed to enter the formal experiment. The formal experiment consists of 5 blocks of 100 trials each, with one-minute break in between. Throughout the experiment, MEG activities were continuously recorded.

Behavioral data analysis

Multiple linear regression model in Experiment 1 (EEG study). To examine what factors contribute to participants' performance (reported location), we fitted a multiple linear regression model to the data (Fig 1B), which was given by:

$$Current\ Report = \beta_1 Current\ Stimulus + \beta_2 Current\ Start + \beta_3 Previous\ Report \quad (1)$$

where "Current Report", "Current Stimulus", and "Current Start" refer to the reported location, the location of the presented item, and the location of the presented mouse cursor in the current trial, respectively, and "Previous Report" is the reported location in the previous trial. For each participant's data, the model was fitted for X and Y coordinates separately and the acquired β_x and β_y were averaged to obtain the regression coefficient for each predictor [14].

The parameter β_3 reflects the serial bias effect. A positive value indicates an attractive effect, i.e., the reported location in the current trial is biased towards the previously reported location, while a negative value corresponds to a repulsive effect.

Linear mixed models (LMM) in Experiment 2 (MEG study). As participants' report accuracy is very high and the reaction time is modulated by the task difficulty (S4 Fig), to quantify their performance in a fine scale, we computed the "weighted choice", by coding their categorical report, as −1 (probe 1) and 1 (probe 2), and then multiplying it by $1 - RT_{rescaled}$, where $RT_{rescaled}$ is the rescaled reaction time in the [0,1] interval. Thus, the "weighted choice", ranges from −1–1, with a value closer to the two bounds indicating a more confident choice.

We next evaluated whether the "weighted choice" can be accounted by six types of locations, which belong to three groups, current stimuli (target and non-target), previous stimuli (target and non-target) and previous choice options (chosen and unchosen). As the task is to compare whether the memorized target location is closer to Probe 1 or Probe 2, distances between the target and respective probes, d_1 and d_2, are calculated, and the decision variable, ΔL, is the distance difference, $d_1 - d_2$. Similarly, ΔL is computed for each of other locations that possibly affect the "weighted choice".

Probe locations could bias decisions by themselves. To evaluate this systematic decision bias, for each pair of probes, we randomly sampled a location within the same 2D round area (15° visual angle in diameter) to compute its ΔL and repeated this procedure 10,000 times to obtain the mean value of ΔL(s). The resulting averaged ΔL reflects the inherent decision bias by the probes, which is further subtracted from the ΔL for each of six candidate locations to obtain the corresponding ΔL_{Demean}.

We fitted linear mixed-effect models to data to examine whether the weighted choice can be predicted by the ΔL_{Demean} of each candidate location. And a full model is given by:

$$weighted\_choice = \beta_0 + \sum_{i=1}^{6} \beta_i \times \Delta L^i_{Demean} \quad (2)$$

where i refers to each of six candidate locations. The regression coefficient β_i represents the influence of one position on current choice, with a positive value indicating attraction and a negative value indicating repulsion. Model performance was evaluated using Akaike information criterion (AIC) with a smaller value indicating better performance. The base model

is the model assuming that the "weighted choice" is only determined by current target location. Models with extra possible combinations of other candidate locations were compared against the base model, and the corresponding ΔAIC was calculated. Note, candidate models were built in a stepwise manner by gradually adding factors that make model perform better (lower AIC). The linear mixed-effect models were performed using fitglme function with "identity" as a link function and all β having a component of random effect in the Matlab Statistics and Machine Learning Toolbox.

Neural data analysis

Neural data acquisition and pre-processing. We used the 64-electrode actiCAP system and two BrainAmp amplifiers with BrainVision Recorder software (Brain Products) to acquire EEG signals in a sound-attenuated, dimly lit, and shielded room. To record the vertical electrooculography, an electrode was positioned below the right eye. The impedance of all electrodes was kept below 15 kΩ. During the recording, the electrode FCz was used as reference, and all signals were sampled at 500 Hz. The EEG data were pre-processed using FieldTrip toolbox [65]. Data were first epoched into single trials from 0.4 s before stimulus onset to 2.5 s after the stimulus onset. The epoched data were re-referenced to the mean signal of all electrodes and then baseline-corrected with the baseline set from 0.4 to 0 s prior to the stimulus onset. Subsequently, EEG data were band-pass filtered within the range of 2–45 Hz, and downsampled to 100 Hz. Within each block, any channel of excessive noise was replaced with the average value of their neighboring channels. Finally, eye-movement related and other artifact components were eliminated from the data using independent component analysis (ICA), guided by visual inspection. No trials were removed during the pre-processing.

The neuromagnetic signal was acquired using a 306-sensor MEG system (102 magnetometers and 204 planar gradiometers, Elekta Neuromag system, Helsinki, Finland) in a sound-attenuated, dimly lit, and shielded room at Peking University. Both horizontal and vertical electrooculograms (EOGs) were recorded. Before each block, we used online head localization to calibrate the participant's head with respect to the MEG sensors. Head movements between blocks must remain within 3 mm for further analysis. The spatiotemporal signal space separation (tSSS) technique implanted in MaxFilter was employed to reduce external noise. The MEG signal was sampled at 1000 Hz. For accurate source localization, structural T1-weighted MRI 1 × 1 × 1 mm^3 resolution) were acquired for each participant on a 3T GE Discovery MR750 MRI scanner (GE Healthcare, Milwaukee, WI, USA). The MEG data were also pre-processed using FieldTrip toolbox [65]. The preprocessing procedure of MEG data is same as what we performed for EEG data except that MEG data were band-pass filtered at 1–40 Hz, and down-sampled to 200 Hz.

Trial-wise representational similarity analysis (RSA). We developed a time-resolved multivariate decoding method, i.e., trial-wise Representational Similarity Analysis [66], to examine neural representations of different types of locations across time. The rationale of this analysis is that neural patterns underlying two locations close to each other are similar and the neural representation similarity decreases as the locations get distant. Linear regression was performed to quantify the relationship between neural representation similarity and location similarity, and the regression coefficient corresponds to the neural representation strength (Fig 2A). Unlike previous studies employing RSA analysis, which typically have discrete stimulus conditions, locations were randomly sampled within a continuous 2D space in both of our experiments. Thus, we calculated the location and neural similarities for each pair of trials, i.e., a trial-wise analysis. Specifically, we computed the Representational Dissimilarity Matrix (RDM) of location separately for the *X* and *Y* axes as follows:

$$RDM\_location_{i,j} = \left| Loc_i - Loc_j \right| \quad (i \neq j) \tag{3}$$

where *i* and *j* are trial indices, and *Loc* represents the *X* or *Y* coordinate of a stimulus' location with the origin being the center of the round area within which stimuli were presented. And at any given time point *t*, the neural RDM is given by:

$$RDM\_neural_{i,j,t} = 1 - \frac{\boldsymbol{V}_{it} \cdot \boldsymbol{V}_{jt}}{\|\boldsymbol{V}_{it}\| \times \|\boldsymbol{V}_{jt}\|} \quad (i \neq j) \tag{4}$$

where $\boldsymbol{V}$ is a vector in the neural representational space at the given time t, and i and j are trial indices. In EEG data analysis, the value of each dimension in $\boldsymbol{V}$ is the EEG signal from a certain channel, and the dimension of $\boldsymbol{V}$ corresponds to the number of EEG channels. In MEG data analysis, we first performed Principal Component Analysis (PCA) on the 306-dimensional signal and kept the smallest number of principle components that explained 99% variance in total (number of components: 59.1 ± 2.60), and the dimension of $\boldsymbol{V}$ corresponds to the number of selected PCA components. In practice, we took advantage of spatiotemporal neural dynamics in a predefined time window (50 ms) to increase decoding performance. Specifically, at each time point, $\boldsymbol{V}$ is determined by pooling neural signals within 50 ms (centered at the given time point) together as a multivariate pattern. To quantify the neural representation strength, for each type of location, we performed a linear regression:

$$RDM\_neural_t = \beta_{0t} + \beta_{1t} \times RDM\_location \tag{5}$$

where β_{0t} is the intercept and β_{1t} is the regression coefficient for the location at time point t. For each participant's data at each time point, we fitted this model for the X and Y axes separately. The neural representation strength of a certain location at a given time point t is obtained by averaging the β_{xt} and β_{yt}. To enhance the decoding sensitivity for previous locations, we regressed out the strong influence of current locations on neural responses and used the residual neural signals for decoding analysis. To ensure that this approach did not introduce any bias, we conducted the same analysis on the target location of the next trial, which yielded nonsignificant decoding performance (S6 Fig).

Past–present interaction analysis. To evaluate how past information interacts with present neural processing, we examined whether the past reactivation shares similarity with the neural representation of current stimulus. In doing so, we computed the representational axes (vectors) for past and present information and then examined their cosine similarity. First, for each EEG/MEG sensor, the signal at each time point was regressed onto past and present locations, resulting in n-dimensional vectors of regression coefficients, i.e., neural representational axes, for all predictors (Figs 2C and 4B). Specifically, for the EEG signals at time point t, we fitted the following model:

$$Sig_{EEG\_t} = \beta_{0t} + \beta_{1t} \times Loc_{current\ stimulus} + \beta_{2t} \times Loc_{current\ start} + \beta_{3t} \times Loc_{previous\ report} \tag{6}$$

where Sig_{EEG_t} is 64-dimensional and Loc denotes the X or Y coordinate for a certain location. The resulting 64-dimensional vectors of β_{1t}, β_{2t}, and β_{3t} are the representational axes for current stimulus, current start and previous report, respectively at time t. For the MEG signals at time t, we fitted the following model:

$$\begin{aligned} Sig_{MEG\_t} = \beta_{0t} &+ \beta_{1t} \times Loc_{current\ target} + \beta_{2t} \times Loc_{current\ non\text{–}target} \\ &+ \beta_{3t} \times Loc_{previous\ choice} + \beta_{4t} \times Loc_{previous\ unchosen} \\ &+ \beta_{5t} \times Loc_{current\ probe1} + \beta_{6t} \times Loc_{current\ probe2} \end{aligned} \tag{7}$$

where Sig_{MEG_t} is the MEG signal from 204 gradiometers at time t and the resulting six 204-dimensional vectors of regression coefficients indicate the corresponding representational axes.

To quantify the past–present interaction, we calculated the cosine similarity between representational axes of previously reported location and that of the current stimulus location. If they are orthogonal (cosine similarity = 0), there would be no interference [35,36]. A negative value indicates that the representational axis of past information is "flipped" in comparison to that of present. Specifically, for a given present location, with the increase of the past location, the activity

on the representational axis of past increases, but the projection from this axis onto the representational axis of present would be decreased due to the "flipped" relationship between these two axes. That is, the increase of past location would cause a decrease of neural response to the present, corresponding to the neural adaptation-like effect or repulsive serial effect [26]. A positive value indicates that past information is "aligned" with the present, corresponding to the attractive serial effect (Figs 2C and 4B).

For each participant's data at each point, we fitted the regression model separately for the *X* and *Y* axes, calculated the respective "past–present interaction," and then averaged them to acquire the overall interaction. The resulting time series of past–present interaction was then smoothed using a 50 ms sliding time window in both the EEG and MEG experiments.

Statistical test for RSA and past–present interaction analyses. For each time period (e.g., encoding) of both experiments, we performed non-parametric sign-permutation test on the time series of "representational strength" and "past–present interaction" to examine whether the variable of interest is significantly different from 0 at the group level [67]. For each permutation, we randomly flipped the sign of the variable being tested from each participant with a 50/50 chance and calculated the group average at each time point. This procedure was repeated 100,000 times to generate a null distribution across time. Next, we compared the original group means against the null distribution at the corresponding time and the *p*-value was calculated as the percentage of values in the null distribution whose absolute values were larger than the actual mean. We then conducted a cluster-based permutation test for multiple comparisons across time, where a cluster was defined based on a threshold of $p = 0.05$.

Neuro-behavioral correlations. To test whether the past–present interaction is related to behavioral serial bias, we performed neuro-behavioral correlations. Specifically, in the EEG experiment, for each participant, the behavioral serial bias was characterized by the regression coefficient of past report (Fig 1B), and the neural effect was quantified by averaging the past–present interaction values across significant time clusters during encoding or decision stage. Pearson correlation was performed to examine the neuro-behavioral correlation across participants. In the MEG experiment, we did not find significant across-participant correlation for past report as Experiment 1 (S2 Fig). This may be attributed to greater individual differences in the perceptual decision-making task than the reproduction task, especially when the effect is primarily reflected in RT. As previous studies revealed that attractive serial dependence could accelerate reactions [20,40], we used RT to index serial dependence effect and calculated within-subject neurobehavioral correlation. The behavioral serial bias was characterized using the reciprocal of reaction time in each trial. For the neural effect, we employed a leave-one-out method to obtain the trial-by-trial past–present interaction. Specifically, for each trial, we fitted a regression model and calculated past–present interactions using all trials except this one. We then derived the trial-level past–present interaction by subtracting the past–present interaction obtained without this trial from the past–present interaction obtained from all trials. The time series of trial-level past–present interactions was smoothed using 50 ms sliding window. Next, we averaged the trial-level past–present interaction values across significant time clusters during the encoding or decision period to get the trial-level neural effect. To quantify the neuro-behavioral relationship, for each participant, we fitted a linear regression model:

$$\textit{behavioral effect} = \beta_0 + \beta_1 \times \textit{neural effect} \tag{8}$$

where β_1 characterizes the neuro-behavioral relationship, with a positive value indicating the behavioral benefit of neural serial dependence, i.e., stronger past–present interactions lead to faster response times.

Sensor Segregation and source localization analyses of MEG data. To investigate the spatial origins of serial dependence, we first conducted sensor segregation analysis on data from both the encoding and decision-making stages. The MEG sensors were split into two halves and the past chosen location decoding and past–present interaction analyses were carried out on each group of sensors separately to investigate whether there is a spatial dissociation between different effects at different stages. Specifically, we divided sensors based on their *Y* position (anterior-posterior

direction) in the 3-D sensor coordinates. Sensors with positive *Y* values are classified as anterior sensors (*N* = 156, 52 magnetometers and 104 gradiometers). Conversely, sensors with negative *Y* values are classified as posterior sensors (*N* = 150, 50 magnetometers and 100 gradiometers).

Next, we conducted source localization analysis to directly examine cortical regions implicated in serial dependence. Similar to the sensor segregation, source analyses were also performed on data from the encoding and decision-making stages. For source reconstruction, we first denoised the pre-processed MEG sensor data using PCA and preserved PCA components that explained 95% variance. Subsequently, the MEG data were co-registered with individual's structural MRI using the MNE_python tool [68], and Boundary Element Method (BEM) models were generated employing the FreeSurfer watershed algorithm [69]. The forward model was then computed utilizing a surface-based source space with 4,096 vertices per hemisphere. Source reconstruction was performed through linear constrained minimum variance (LCMV) beamforming [70] with a regularization parameter set as 5%, the noise matrix characterized by the baseline data, 0–400 ms before stimulus onset, and data matrices of the encoding and decision-making stages were computed based on the corresponding stage's data. Then, MEG sources were anatomically mapped to 34 regions of interest encompassing both left and right hemispheres based on the Desikan–Killiany atlas [41]. We combined left and right hemispheres together and conducted the decoding and past–present interaction analyses on each region, just as what we did in sensor analyses but treated a voxel as a sensor here. To address multi-comparison issue across cortical regions, temporal clusters in each region were compared against permuted clusters across all regions, resulting in a spatially corrected *p* value.

Supporting information

S1 Table. Behavioral model comparison of Experiment 2, related to Fig 3.
(XLSX)

S1 Fig. Time-resolved grand average of past–present interactions between current target and previous unchosen location in Experiment 2 (MEG), related to Fig 4. The shaded areas correspond to ±1 SEM. Positive and negative values correspond to aligned and flipped direction, respectively. Horizontal lines denote significant temporal clusters (cluster-based permutation test, $p < 0.05$, two-sided, corrected). Data supporting this figure can be found at: https://osf.io/c7dwp/.
(DOCX)

S2 Fig. Across-participant neuro-behavioral correlation in Experiment 2 (MEG), related to Fig 4. (A). Cross-subject correlation between serial dependence behavior (*x*-axis; regression coefficient) and past–present neural interaction (*y*-axis; averaged within significant clusters) induced by previous chosen location during Encoding (purple) and Decision-making (blue) stages. **(B)**. The same as **A** but for serial dependence behavior and past–present neural interaction induced by previous unchosen location during Encoding stage. Each dot represents individual participant. The solid lines correspond to the best linear fitting, and the shaded areas correspond to 95% confidence interval. Data supporting this figure can be found at: https://osf.io/c7dwp/.
(DOCX)

S3 Fig. Time courses of 2-stage cortical origins of serial biases in all significant regions in Experiment 2 (MEG), related to Fig 5. (A). Time-resolved grand averaged decoding results of previous chosen location during encoding stage. The regions of significant temporal clusters displayed on the inflated cortical surface and their names are shown at the leftmost. Dark and light colors denote temporal clusters with or without spatial correction. Except Cuneus (shown in Fig 5), time courses of all regions with significant temporal clusters are plotted. **(B)**. Same as **A** but for the past–present interactions. **(C,D)**. Same as **AB** but during decision-making stages. Panel **C** does not include the result of medial OFC and

panel **D** does not include pars orbitalis. The shaded areas correspond to ±1 SEM. Color-coded horizontal lines denote significant temporal clusters (cluster-based permutation test, $p < 0.05$, two-sided, corrected). Data supporting this figure can be found at: https://osf.io/c7dwp/.
(DOCX)

S4 Fig. Reaction time (*Y*-axis) as a function of distance difference (*X*-axis) in Experiment 2, related to Methods. The grey lines indicate the best linear fitting for each subject and the black line is the best fitting across all subjects. Data supporting this figure can be found at: https://osf.io/c7dwp/.
(DOCX)

S5 Fig. Neural bias in present location representations caused by previous reported location. Using leave-one-out method, we trained a linear decoder to reconstruct present locations by employing a multiple linear regression model and tested whether it could be predicted by previous reported location. The neural bias is characterized by the regression coefficient. **(A)** Time-resolved grand averaged neural bias in Experiment 1. Location reconstruction is based on neural activities on all EEG sensors. **(B)** Time-resolved grand averaged neural bias in Experiment 2 (sensor level). Location reconstruction is based on neural activities from all MEG sensors. **(C,D)** Time-resolved grand averaged neural bias during encoding in Cuneus and decision-making in Pars orbitalis. The shaded areas correspond to ±1 SEM. Color-coded horizontal lines denote significant temporal clusters (cluster-based permutation test, $p < 0.05$, one-sided, corrected). Data supporting this figure can be found at: https://osf.io/c7dwp/.
(DOCX)

S6 Fig. Neural decoding of information in the current and next trials (Experiment 2). When decoding information in the next trial, we regressed out the influence of current locations from neural signals and used the residuals. The shaded areas correspond to ±1 SEM. Color-coded horizontal lines denote significant temporal clusters (cluster-based permutation test, $p < 0.05$, two-sided, corrected). Data supporting this figure can be found at: https://osf.io/c7dwp/.
(DOCX)

Acknowledgments

We thank the Center for MRI Research at Peking University for assistance with data acquisition.

Author contributions

Conceptualization: Minghao Luo, Huihui Zhang, Huan Luo.

Data curation: Minghao Luo.

Formal analysis: Minghao Luo, Huihui Zhang.

Funding acquisition: Huihui Zhang, Fang Fang, Huan Luo.

Methodology: Minghao Luo, Huihui Zhang.

Project administration: Huihui Zhang, Huan Luo.

Resources: Fang Fang, Huan Luo.

Supervision: Huihui Zhang, Fang Fang, Huan Luo.

Validation: Huan Luo.

Visualization: Minghao Luo, Huihui Zhang.

Writing – original draft: Minghao Luo, Huihui Zhang, Huan Luo.

Writing – review & editing: Minghao Luo, Huihui Zhang, Fang Fang, Huan Luo.

References

1. Dong DW, Atick JJ. Statistics of natural time-varying images. Comput Neural Sys. 1995;6:345–58.
2. Voss RF, Clarke J. 1-F-Noise in Music and Speech. Nature. 1975;258:317–8.
3. Gold JI, Stocker AA. Visual decision-making in an uncertain and dynamic world. Annu Rev Vis Sci. 2017;3:227–50. https://doi.org/10.1146/annurev-vision-111815-114511 PMID: 28715956.
4. Fischer J, Whitney D. Serial dependence in visual perception. Nat Neurosci. 2014;17:738–43.
5. Cicchini GM, Mikellidou K, Burr DC. Serial dependence in perception. Annu Rev Psychol. 2024;75:129–54. https://doi.org/10.1146/annurev-psych-021523-104939 PMID: 37758238.
6. Manassi M, Murai Y, Whitney D. Serial dependence in visual perception: a meta-analysis and review. J Vis. 2023;23:18. https://doi.org/10.1167/jov.23.8.18 PMID: 37642639.
7. Pascucci D, Tanrikulu ÖD, Ozkirli A, Houborg C, Ceylan G, Zerr P, et al. Serial dependence in visual perception: a review. J Vis. 2023;23(1):9. https://doi.org/10.1167/jov.23.1.9 PMID: 36648418.
8. Kiyonaga A, Scimeca JM, Bliss DP, Whitney D. Serial dependence across perception, attention, and memory. Trends Cogn Sci. 2017;21:493–7. https://doi.org/10.1016/j.tics.2017.04.011 PMID: 28549826.
9. Cicchini GM, Mikellidou K, Burr D. Serial dependencies act directly on perception. J Vis. 2017;17.
10. Fritsche M, Mostert P, de Lange FP. Opposite effects of recent history on perception and decision. Curr Biol. 2017;27(4):590–5. https://doi.org/10.1016/j.cub.2017.01.006 PMID: 28162897.
11. Pascucci D, Mancuso G, Santandrea E, Della Libera C, Plomp G, Chelazzi L. Laws of concatenated perception: vision goes for novelty, decisions for perseverance. PLOS Biol. 2019;17:e3000144. https://doi.org/10.1371/journal.pbio.3000144 PMID: 30835720.
12. Zhang H, Alais D. Individual difference in serial dependence results from opposite influences of perceptual choices and motor responses. J Vis. 2020;20(2):2–2. PMID: 32744618.
13. Cicchini GM, Anobile G, Burr DC. Compressive mapping of number to space reflects dynamic encoding mechanisms, not static logarithmic transform. Proc Natl Acad Sci U S A. 2014;111:7867–72. https://doi.org/10.1073/pnas.1402785111 PMID: 24821771.
14. Luo M, Zhang H, Luo H. Cartesian coordinates scaffold stable spatial perception over time. J Vis. 2022;22:13. https://doi.org/10.1167/jov.22.8.13 PMID: 35857298.
15. Manassi M, Liberman A, Kosovicheva A, Zhang K, Whitney D. Serial dependence in position occurs at the time of perception. Psychon Bull Rev. 2018;25(6):2245–53. https://doi.org/10.3758/s13423-018-1454-5 PMID: 29582377.
16. Taubert J, Van der Burg E, Alais D. Love at second sight: sequential dependence of facial attractiveness in an on-line dating paradigm. Sci Rep. 2016;6.
17. Motala A, Zhang HH, Alais D. Auditory rate perception displays a positive serial dependence. I-perception. 2020;11.
18. Zhang H, Luo H. Feature-specific reactivations of past information shift current neural encoding thereby mediating serial bias behaviors. PLOS Biol. 2023;21:e3002056. https://doi.org/10.1371/journal.pbio.3002056 PMID: 36961821.
19. Manassi M, Whitney D. Continuity fields enhance visual perception through positive serial dependence. Nat Rev Psychol. 2024;3(5):352–66.
20. Cicchini GM, Mikellidou K, Burr DC. The functional role of serial dependence. P Roy Soc B-Biol Sci. 2018;285.
21. Manassi M, Whitney D. Illusion of visual stability through active perceptual serial dependence. Sci Adv. 2022;8(2):eabk2480. https://doi.org/10.1126/sciadv.abk2480 PMID: 35020432.
22. Fritsche M, Spaak E, de Lange FP. A Bayesian and efficient observer model explain concurrent attractive and repulsive history biases in visual perception. Elife. 2020;9:e55389. https://doi.org/10.7554/eLife.55389 PMID: 32479264.
23. Cicchini GM, Benedetto A, Burr DC. Perceptual history propagates down to early levels of sensory analysis. Curr Biol. 2020.
24. Ceylan G, Herzog MH, Pascucci D. Serial dependence does not originate from low-level visual processing. Cognition. 2021;212:104709. https://doi.org/10.1016/j.cognition.2021.104709 PMID: 33838523.
25. John-Saaltink ES, Kok P, Lau HC, de Lange FP. Serial dependence in perceptual decisions is reflected in activity patterns in primary visual cortex. J Neurosci. 2016;36:6186–92.
26. Hajonides JE, van Ede F, Stokes MG, Nobre AC, Myers NE. Multiple and dissociable effects of sensory history on working-memory performance. J Neurosci. 2023;43(15):2730–40. https://doi.org/10.1523/JNEUROSCI.1200-22.2023 PMID: 36868858.
27. Sheehan TC, Serences JT. Attractive serial dependence overcomes repulsive neuronal adaptation. PLoS Biol. 2022;20:e3001711. https://doi.org/10.1371/journal.pbio.3001711 PMID: 36067148.
28. Barbosa J, Stein H, Martinez RL, Galan-Gadea A, Li S, Dalmau J, et al. Interplay between persistent activity and activity-silent dynamics in the prefrontal cortex underlies serial biases in working memory. Nat Neurosci. 2020;23:1016–24.
29. Akrami A, Kopec CD, Diamond ME, Brody CD. Posterior parietal cortex represents sensory history and mediates its effects on behaviour. Nature. 2018;554:368–72.

30. Neto RMD, Bartels A. Disrupting short-term memory maintenance in premotor cortex affects serial dependence in visuomotor integration. J Neurosci. 2021;41:9392–402. https://doi.org/10.1523/JNEUROSCI.0380-21.2021 PMID: 34607968.
31. Bae G-Y, Luck SJ. Reactivation of previous experiences in a working memory task. Psychol Sci. 2018;30:587–95.
32. Fornaciai M, Park J. Attractive serial dependence in the absence of an explicit task. Psychol Sci. 2017;29:437–446. https://doi.org/10.1177/0956797617737385 PMID: 29381415.
33. Ranieri G, Benedetto A, Ho HT, Burr DC, Morrone MC. Evidence of serial dependence from decoding of visual evoked potentials. J Neurosci. 2022;42:8817–25. https://doi.org/10.1523/JNEUROSCI.1879-21.2022 PMID: 36223998.
34. Luo J, Collins T. The representational similarity between visual perception and recent perceptual history. J Neurosci. 2023;43(20):3658–65. https://doi.org/10.1523/JNEUROSCI.2068-22.2023 PMID: 36944487.
35. Bouchacourt F, Buschman TJ. A flexible model of working memory. Neuron. 2019;103(1):147–60. https://doi.org/10.1016/j.neuron.2019.04.020 PMID: 31103359.
36. Whittington JC, Dorrell W, Behrens TE, Ganguli S, El-Gaby M. A tale of two algorithms: structured slots explain prefrontal sequence memory and are unified with hippocampal cognitive maps. Neuron. 2025;113(2):321–33.
37. Xie Y, Hu P, Li J, Chen J, Song W, Wang XJ, et al. Geometry of sequence working memory in macaque prefrontal cortex. Science. 2022;375(6581):632–9. https://doi.org/10.1126/science.abm0204 PMID: 35143322.
38. Libby A, Buschman TJ. Rotational dynamics reduce interference between sensory and memory representations. Nat Neurosci. 2021;1–12.
39. Weber J, Iwama G, Solbakk A-K, Blenkmann AO, Larsson PG, Ivanovic J, et al. Subspace partitioning in the human prefrontal cortex resolves cognitive interference. Proc Natl Acad Sci U S A. 2023;120(28):e2220523120. https://doi.org/10.1073/pnas.2220523120 PMID: 37399398.
40. Urai AE, de Gee JW, Tsetsos K, Donner TH. Choice history biases subsequent evidence accumulation. Elife. 2019;8:e46331. https://doi.org/10.7554/eLife.46331 PMID: 31264959.
41. Desikan RS, Ségonne F, Fischl B, Quinn BT, Dickerson BC, Blacker D, et al. An automated labeling system for subdividing the human cerebral cortex on MRI scans into gyral based regions of interest. Neuroimage. 2006;31(3):968–80. https://doi.org/10.1016/j.neuroimage.2006.01.021 PMID: 16530430.
42. Whitney D, Manassi M, Murai Y. Searching for serial dependencies in the brain. PLoS Biol. 2022;20:e3001788. https://doi.org/10.1371/journal.pbio.3001788 PMID: 36070292.
43. Wei XX, Stocker AA. A Bayesian observer model constrained by efficient coding can explain "anti-Bayesian" percepts. Nat Neurosci. 2015;18(10):1509–1517. https://doi.org/10.1038/nn.4105 PMID: 26343249.
44. Fritsche M, Solomon SG, de Lange FP. Brief stimuli cast a persistent long-term trace in visual cortex. J Neurosci. 2022;42(10):1999–2010. https://doi.org/10.1523/JNEUROSCI.1350-21.2021 PMID: 35064003.
45. Fornaciai M, Park J. Spontaneous repulsive adaptation in the absence of attractive serial dependence. J Vis. 2019;19(5):21. https://doi.org/10.1167/19.5.21 PMID: 31112999.
46. Rideaux R, West RK, Rangelov D, Mattingley JB. Distinct early and late neural mechanisms regulate feature-specific sensory adaptation in the human visual system. Proc Natl Acad Sci USA. 2023;120:6.
47. Urai AE, Donner TH. Persistent activity in human parietal cortex mediates perceptual choice repetition bias. Nat Commun. 2022;13:6015. https://doi.org/10.1038/s41467-022-33237-5 PMID: 36224207.
48. Schwiedrzik CM, Ruff CC, Lazar A, Leitner FC, Singer W, Melloni L. Untangling perceptual memory: hysteresis and adaptation map into separate cortical networks. Cereb Cortex. 2014;24:1152–64.
49. Cheng S, Chen SY, Glasauer S, Keeser D, Shi ZH. Neural mechanisms of sequential dependence in time perception: the impact of prior task and memory processing. Cereb Cortex. 2023.
50. Mochol G, Kiani R, Moreno-Bote R. Prefrontal cortex represents heuristics that shape choice bias and its integration into future behavior. Curr Biol. 2021;31:1234–44.e1236.
51. Nogueira R, Abolafia JM, Drugowitsch J, Balaguer-Ballester E, Sanchez-Vives MV, Moreno-Bote R. Lateral orbitofrontal cortex anticipates choices and integrates prior with current information. Nat Commun. 2017;8:14823. https://doi.org/10.1038/ncomms14823 PMID: 28337990.
52. Forstmann BU, Brown S, Dutilh G, Neumann J, Wagenmakers EJ. The neural substrate of prior information in perceptual decision making: a model-based analysis. Front Hum Neurosci. 2010;4:40. https://doi.org/10.3389/fnhum.2010.00040 PMID: 20577592.
53. Fischer C, Czoschke S, Peters B, Rahm B, Kaiser J, Bledowski C. Context information supports serial dependence of multiple visual objects across memory episodes. Nat Commun. 2020;11:1932. https://doi.org/10.1038/s41467-020-15874-w PMID: 32321924.
54. Shan J, Hajonides JE, Myers NE. Neural evidence for decision-making underlying attractive serial dependence. bioRxiv. 2024;2024-11.
55. Fischer C, Kaiser J, Bledowski C. A direct neural signature of serial dependence in working memory. Elife. 2024;13:RP99478.
56. Stokes MG. "Activity-silent" working memory in prefrontal cortex: a dynamic coding framework. Trends Cogn Sci. 2015;19(7):394–405. https://doi.org/10.1016/j.tics.2015.05.004 PMID: 26051384.
57. Sun Q, Zhan L-Z, Zhang B-Y, Jia S, Gong X-M. Heading perception from optic flow occurs at both perceptual representation and working memory stages with EEG evidence. Vision Res. 2023;208:108235. https://doi.org/10.1016/j.visres.2023.108235 PMID: 37094419.

58. Christophel TB, Klink PC, Spitzer B, Roelfsema PR, Haynes JD. The distributed nature of working memory. Trends Cogn Sci. 2017;21:111–24.
59. Serences JT, Ester EF, Vogel EK, Awh E. Stimulus-specific delay activity in human primary visual cortex. Psychol Sci. 2009;20(2):207–14. https://doi.org/10.1111/j.1467-9280.2009.02276.x PMID: 19170936.
60. Kwak Y, Curtis CE. Unveiling the abstract format of mnemonic representations. Neuron. 2022;110:1822–28. https://doi.org/10.1016/j.neuron.2022.03.016 PMID: 35395195.
61. Rademaker R, Chunharas C, Serences J. Coexisting representations of sensory and mnemonic information in human visual cortex. Nat Neurosci. 2019;22(8):1336–44. https://doi.org/10.1038/s41593-019-0428-x PMID: 31263205.
62. Schuck NW, Cai MB, Wilson RC, Niv Y. Human orbitofrontal cortex represents a cognitive map of state space. Neuron. 2016;91(6):1402–12. https://doi.org/10.1016/j.neuron.2016.08.019 PMID: 27657452.
63. Kim S, Burr D, Cicchini GM, Alais D. Serial dependence in perception requires conscious awareness. Curr Biol. 2020;30:R257–8.
64. Brainard DH. The psychophysics toolbox. Spat Vis. 1997;10:433–6. PMID: 9176952.
65. Oostenveld R, Fries P, Maris E, Schoffelen J-M. FieldTrip: Open source software for advanced analysis of MEG, EEG, and invasive electrophysiological data. Comput Intell Neurosci. 2011;2011:156869. https://doi.org/10.1155/2011/156869 PMID: 21253357.
66. Kriegeskorte N, Mur M, Bandettini P. Representational similarity analysis - connecting the branches of systems neuroscience. Front Syst Neurosci. 2008;2:4. https://doi.org/10.3389/neuro.06.004.2008 PMID: 19104670.
67. Maris E, Oostenveld R. Nonparametric statistical testing of EEG- and MEG-data. J Neurosci Methods. 2007;164:177–90. https://doi.org/10.1016/j.jneumeth.2007.03.024 PMID: 17517438.
68. Gramfort A, Luessi M, Larson E, Engemann DA, Strohmeier D, Brodbeck C, et al. MNE software for processing MEG and EEG data. Neuroimage. 2014;86:446–60. https://doi.org/10.1016/j.neuroimage.2013.10.027 PMID: 24161808.
69. Ségonne F, Dale AM, Busa E, Glessner M, Salat D, Hahn HK, et al. A hybrid approach to the skull stripping problem in MRI. Neuroimage. 2004;22:1060–75.
70. VanVeen BD, vanDrongelen W, Yuchtman M, Suzuki A. Localization of brain electrical activity via linearly constrained minimum variance spatial filtering. IEEE T Bio-Med Eng. 1997;44:867–80.